

Microstructure evolution and nucleation mechanism of Inconel 601H alloy welds by vibration-assisted GTAW

Ze-long Wang¹⁾, Zhen-tai Zheng¹⁾, Li-bing Zhao¹⁾, Yun-feng Lei¹⁾, and Kun Yang²⁾

1) School of Materials Science and Engineering, Hebei University of Technology, Tianjin 300130, China

2) Beiyang Chemical Equipment of Tianjin University Co., Ltd., Tianjin 300110, China

(Received: 10 November 2017; revised: 17 March 2018; accepted: 20 March 2018)

Abstract: Nickel-based alloys exhibit excellent high-temperature strength and oxidation resistance; however, because of coarse grains and severe segregation in their welding joints, these alloys exhibit increased susceptibility to hot cracking. In this paper, to improve the hot-cracking resistance and mechanical properties of nickel-based alloy welded joints, sodium thiosulfate was used to simulate crystallization, enabling the nucleation mechanism under mechanical vibration to be investigated. On the basis of the results, the grain refinement mechanism during the gas tungsten arc welding (GTAW) of Inconel 601H alloy under various vibration modes and parameters was investigated. Compared with the GTAW process, the low-frequency mechanical vibration processes resulted in substantial grain refinement effects in the welds; thus, a higher hardness distribution was also achieved under the vibration conditions. In addition, the γ' phase exhibited a dispersed distribution and segregation was improved in the welded joints with vibration assistance. The results demonstrated that the generation of free crystals caused by vibration in the nucleation stage was the main mechanism of grain refinement. Also, fine equiaxed grains and a dispersed γ' phase were found to improve the grain-boundary strength and reduce the segregation, contributing to preventing the initiation of welding hot cracking in nickel-based alloys.

Keywords: mechanical vibration; nickel-based alloy; grain refinement; microstructure; hot cracking

1. Introduction

Nickel-based alloys exhibit excellent high-temperature strength, oxidation resistance, corrosion resistance, and microstructure stability. Therefore, these alloys play important roles in aerospace engines and industrial gas turbines. However, the welding joints of nickel-based alloys are prone to severe segregation, grain coarsening, and hot cracking when welded using conventional welding processes [1]. To improve the weld quality of nickel-based alloys, mechanical vibration can be used to apply periodic excitation force to the weldment during welding and influence the solidification process of the weld pool, thereby leading to grain refinement and the suppression of welding defects [2–6]. This welding process is called vibration-assisted welding. Vibration-assisted welding has already achieved excellent results in the welding of stainless steel [7–8] and aluminum alloy [9–11].

Fine grains help reduce the susceptibility of the weld metal to solidification cracking during welding. Dai [12] and Watanabe *et al.* [7] introduced ultrasonic vibration into weld pools and obtained a fine equiaxed dendritic microstructure in the weld metal. Liu and Wu [13–14] used ultrasonic-vibration-enhanced friction stir welding (UVEFSW) to weld aluminum alloy. The ultrasonic vibration effectively enhanced the liquid metal flow in the mixing zone, eliminated welding defects and improved the weld quality. However, the microstructures of the UVEFSW joints exhibit through-thickness microstructure inhomogeneity arising mainly from the variable thermomechanical interaction of the friction stir welding tool with the workpiece. Ultrasonic vibration has other disadvantages, including large attenuation and high equipment costs. Furthermore, transferring ultrasonic vibration into the weld pool is technically difficult. By comparison, not only can low-frequency mechanical vibration achieve the same grain refinement effect during

Corresponding author: Zhen-tai Zheng E-mail: zzt@hebut.edu.cn

© University of Science and Technology Beijing and Springer-Verlag GmbH Germany, part of Springer Nature 2018

welding, but the equipment is simple and practical. Kou and Le [15] pointed out that low-frequency mechanical vibration can reduce hot cracking and refine the grain in welds. Kuo *et al.* [8] applied low-frequency mechanical vibration during the gas tungsten arc welding (GTAW) of stainless steel. The vibration weld presented a very small δ -ferrite structure, a uniform composition distribution, and little residual stress. Wu [16] studied the effect of low-frequency mechanical vibration on the weld metal of nickel 690 alloy and found that the grain size decreased and the dendrite orientation became not obvious; however, he did not further analyze the grain refinement mechanism. The aforementioned research results indicate that low-frequency mechanical vibration is more efficient than ultrasonic vibration for improving weld quality.

The underlying mechanism of the coupling interaction between the mechanical vibration energy and the solidification of a weld pool remains unclear. Grain refinement is generally accepted as being caused by dendrite fragmentation, which can occur through two mechanisms: solute segregation and recalescence [17–19]. In the process of mechanical-vibration-assisted welding, vibrational energy with strong shear force can break dendrites directly. However, dendrites can also undergo plastic deformation during the solidification process, and inducing dendrite fragmentation using only mechanical loading is difficult, especially for nickel-based alloys with excellent high-temperature strength. Hellawell *et al.* [20] demonstrated that dendrite fragmentation by mechanical breakup of dendrite arms was highly unlikely. Reheating and growth-rate fluctuations could both cause dendrite fragmentation by remelting of dendrite

arms [21]. Thus far, scholars who investigate mechanical-vibration-assisted welding have focused on the dendrite fragmentation mechanism throughout the grain growth stage. By contrast, the literature contains no reports of theoretical analyses of the nucleation stage of the weld pool under low-frequency mechanical vibration.

In this study, through comparative experiments on a transparent $\text{Na}_2\text{S}_2\text{O}_3 \cdot 5\text{H}_2\text{O}$ model and a metal Inconel 601H alloy, we attempt to provide a generalized explanation of the grain refinement mechanism of a weld under low-frequency mechanical vibration. Directly observing the solidification process of the weld pool is difficult. By contrast, the transparent model can be observed directly and exhibits solidification features similar to those of metals. A reasonable explanation of the grain refinement mechanism is achieved by combining the results of these two experiments. In addition, the microstructures and precipitation phases of welds under various vibration modes and parameters were studied and the hardness of the welding joints was analyzed.

2. Experimental

2.1. Vibration platform

In these experiments, a mechanical vibration motor with a vibration frequency of 50 Hz and a maximum exciting force of 1.96 kN was used as the exciter. During the vibration process, the output power was approximately 250 W. The exciter generated periodic excitation force by rotating the eccentric block, causing the specimen fixed on the platform to produce low-frequency mechanical vibration. Fig. 1 shows the vibration-assisted welding system.

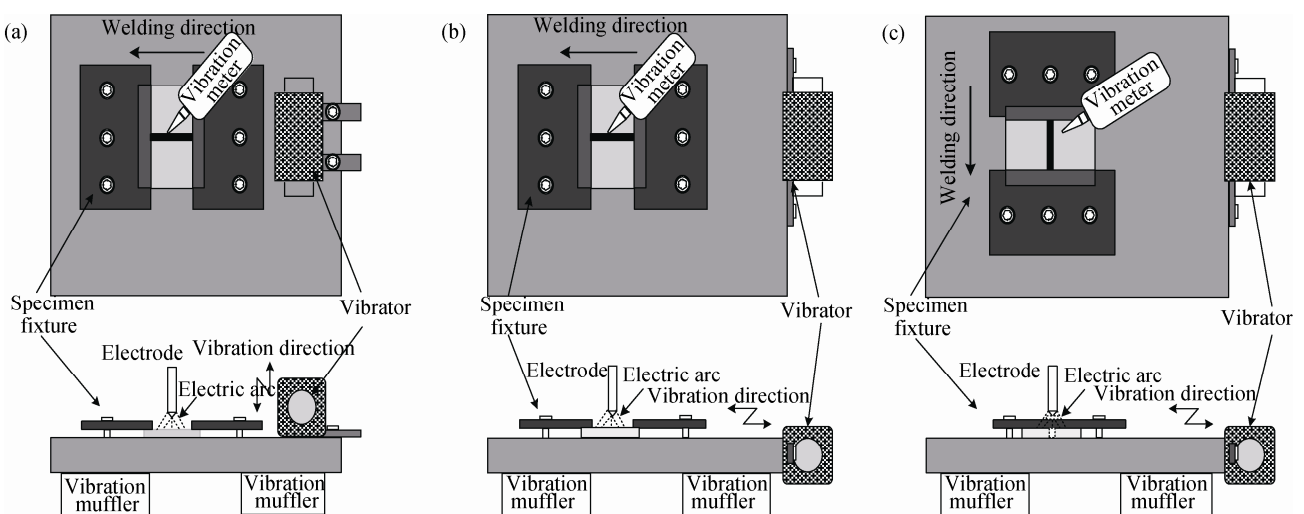


Fig. 1. Vibration-assisted welding system: (a) V-vib; (b) LFH-vib; (c) TFH-vib.

As shown in Fig. 1, the vertical vibration (V-vib) and the horizontal vibration (H-vib) could be superimposed on

weldments during GTAW. In the V-vib experiments, the exciter caused the weldment to produce reciprocating move-

ment in the direction perpendicular to the plane of the platform, as shown in Fig. 1(a). In the H-vib experiments, the exciter caused the weldment to produce reciprocating movement in the direction parallel to the plane of the platform. Because of the differences in the relative positions between the weldment and the exciter, the forced direction of the weld pool also changed, which would inevitably affect the solidification process. Therefore, the longitudinal fixation horizontal vibration (LFH-vib) and transverse fixation horizontal vibration (TFH-vib) were selected, as shown in Figs. 1(b) and 1(c), respectively. In the LFH-vib experiments, the weld pool was subjected to reciprocating movement parallel to the welding direction. In the TFH-vib experiments, the weld pool was subjected to reciprocating movement perpendicular to the welding direction. Prior to the experiments, the exciter was opened for 2 min to allow the vibration to stabilize. The magnitude of the vibration amplitude was adjusted by changing the distance between the weldment and the exciter. The vibration amplitude of weldment was measured using a vibration meter before welding.

2.2. Physical simulation

The transparent crystal used in the physical simulation experiment was sodium thiosulfate ($\text{Na}_2\text{S}_2\text{O}_3 \cdot 5\text{H}_2\text{O}$); the liquidus temperature was 48°C. In the experiments, sodium

thiosulfate crystals were placed into a beaker, which was subsequently heated using an alcohol lamp. When the sodium thiosulfate was heated to 52°C (4°C above the liquidus temperature) and had completely changed into liquid, the liquid was poured into a culture dish with a diameter of 60 mm. The depth of the liquid was 3 mm. The culture dish was then fixed on the vibration platform, and vertical and horizontal vibrations were applied. The vibration amplitude was maintained at approximately 0.2 mm. A digital camera was used to record the liquid crystallization process in the culture dish.

2.3. Vibration-assisted welding

In this study, Inconel 601H alloy was used as the experimental material and specimens with dimensions of 80 mm × 100 mm × 3 mm were welded automatically. Inconel 601H alloy is a solid-solution-strengthened alloy with aluminum and titanium additives. The chemical composition of Inconel 601H alloy is given in Table 1.

In the vibration-assisted welding process, automatic GTAW welding without filler metal was used. A series of experiments revealed that fierce fluctuation of the weld pool would lead to poor weld formation when the vibration amplitude exceeded 0.2 mm. Thus, the maximum vibration amplitude was 0.2 mm; the welding and vibration parameters used in these experiments are shown in Tables 2 and 3, respectively.

Table 1. The chemical composition of Inconel 601H alloy

wt%

Ni	Cr	Fe	C	Mn	Si	Cu	Al	Ti*	P*	S
58.0–63.0	21.0–25.0	Bal.	≤0.10	≤1.5	≤0.5	≤1.0	1.0–1.7	0.3–0.5	≤0.020	≤0.015

Note: *—not specified in ASTM.

Table 2. Welding parameters

Welding current / A	Arc voltage / V	Travel speed / ($\text{mm} \cdot \text{s}^{-1}$)	Argon flow rate / ($\text{L} \cdot \text{min}^{-1}$)
140	12	150	12

Table 3. Vibration parameters

Vibration mode	Vibration amplitude / mm	Vibration frequency / Hz
V-vib	0.1	50
	0.15	
	0.2	
LFH-vib	0.1	50
	0.15	
	0.2	
TFH-vib	0.1	50
	0.15	
	0.2	

The welding joints were sliced using wire-electrode cutting, and the standard procedure was used to prepare metallographic samples. A Leica DM2700 optical microscope and a HITACHI S-4800 scanning electron microscope equipped with an EDAX energy-dispersive spectroscopy (EDS) apparatus were used to analyze the microstructure and segregation. X-ray diffraction (XRD) (Bruker D8 Discover) was used to analyze the phase composition. A Shimadzu HVM-2T Vickers hardness tester was used to measure the hardness under a test load of 50 g for a dwell time of 10 s.

3. Results and discussion

3.1. Effect of vibration amplitude on the microstructure of weld

The microstructures of the welds obtained at vibration

amplitudes of 0 mm, 0.1 mm, 0.15 mm, and 0.2 mm with V-vib, LFH-vib, and TFH-vib are shown in Figs. 2–4, respectively. In the absence of vibration, coarse columnar grains ex-

isted throughout the fusion zone, as shown in Fig. 2(a). By contrast, the vibration amplitude increased from 0.1 to 0.15 and 0.2 mm, the effect of grain refinement increased gradually.

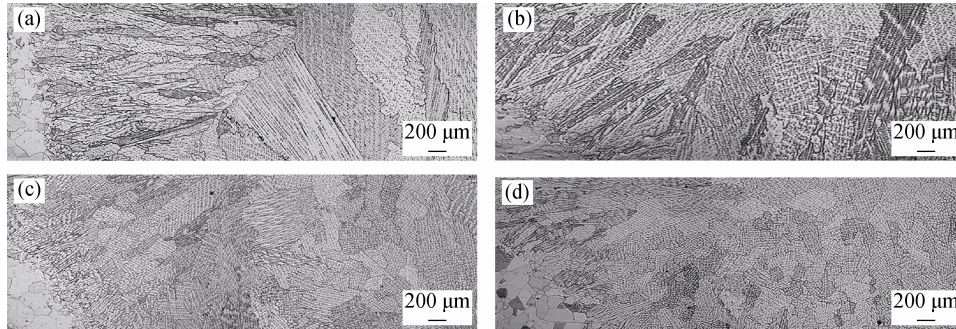


Fig. 2. Microstructures of welds with different amplitudes under V-vib: (a) 0 mm; (b) 0.1 mm; (c) 0.15 mm; (d) 0.2 mm.

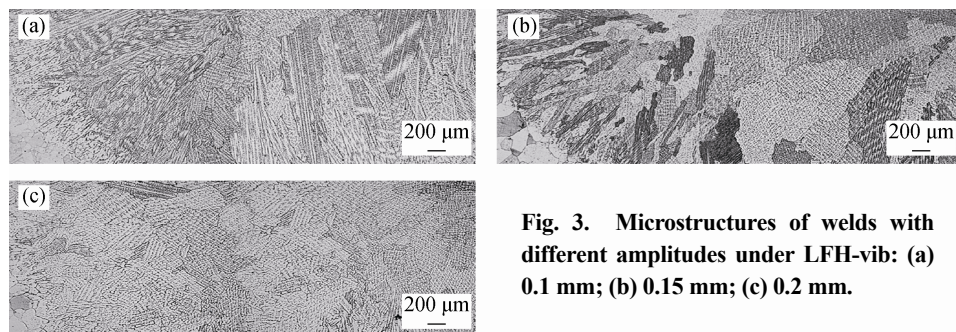


Fig. 3. Microstructures of welds with different amplitudes under LFH-vib: (a) 0.1 mm; (b) 0.15 mm; (c) 0.2 mm.

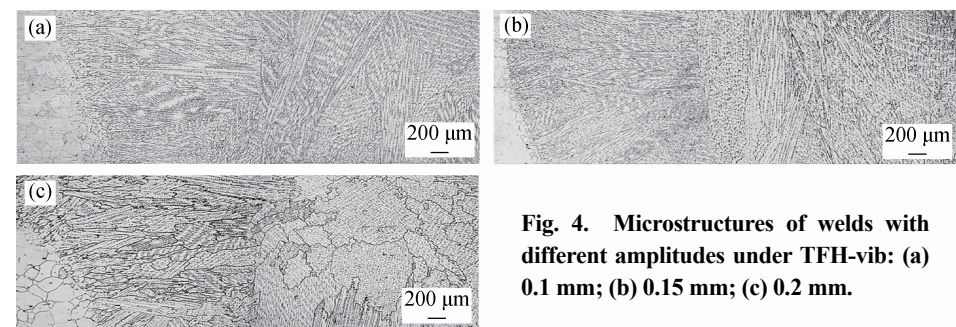


Fig. 4. Microstructures of welds with different amplitudes under TFH-vib: (a) 0.1 mm; (b) 0.15 mm; (c) 0.2 mm.

At the 0.1 mm vibration amplitude, the grain sizes of the welds remained basically unchanged. This observation is attributed to low vibrational energy, which results in a diminished effect on the weld pool. From the V-vib and LFH-vib welds at 0.15 mm amplitude, the grain size begins to decrease and visible grain refinements are observed near the weld center, as shown in Figs. 2(c) and 3(b). Nevertheless, the effect of vibration on the TFH-vib weld is insignificant at this amplitude, a coarser microstructure is still obtained in the fusion zone, as shown in Fig. 4(b). The grain refinement of Inconel 601H alloy clearly has an amplitude threshold related to the vibration modes. A further increase in amplitude to 0.2 mm revealed that the V-vib and LFH-vib welds are mainly

composed of fine equiaxed grains, as shown in Figs. 2(d) and 3(c), respectively. However, the LFH-vib weld is mainly composed of coarse columnar grains and a small amount of equiaxed grains, as shown in Fig. 4(c). Through further comparison, we discovered that the effect of grain refinement changes with various vibration modes at the same amplitude. This behavior is possibly related to the convection differences caused by the vibration modes within the weld pool.

3.2. Identification of grain refinement mechanism

Inoculation is unlikely to be the mechanism of grain refinement because no welding filler was used in the vibration-assisted welding. Therefore, vibration is predominantly

responsible for grain refinement. In fact, scholars have demonstrated that dendrite remelting induced by reheating and by growth-rate fluctuations was the main reason for grain refinement [21]. However, the TFH-vib weld was influenced by vibration but showed no obvious grain refinement effect. This result suggests that the dendrite remelting hypothesis at the stage of grain growth does not apply to Inconel 601H alloy. Thus, we began our study of the grain refinement mechanism from the perspective of the nucleation stage of the weld pool.

3.2.1. Effect of vibration on boundary layer

Fig. 5 shows the physical simulation results for sodium thiosulfate under vibration. The crystallization processes under natural, V-vib, and H-vib conditions are shown in Figs.

5(a)–5(c), respectively. Figs. 5(a1), 5(b1), and 5(c1) corresponds to the beginning of crystallization. Figs. 5(a2), 5(b2), and 5(c2) corresponds to the initial stage of crystallization. Figs. 5(a3), 5(b3), and 5(c3) corresponds to the middle stage of crystallization. Figs. 5(a4), 5(b4), and 5(c4) corresponds the end of crystallization. As evident in Fig. 5(a1), the primary crystals form in the middle and at the wall of the culture dish at the beginning of natural crystallization. In Figs. 5(a2) and 5(a3), the crystals around the wall are observed to grow in the form of columnar crystals, whereas the crystals in the middle of the culture dish are observed to grow in the form of equiaxed crystals. The crystal morphology is eventually dominated by coarse columnar crystals and equiaxed crystals, as shown in Fig. 5(a4).

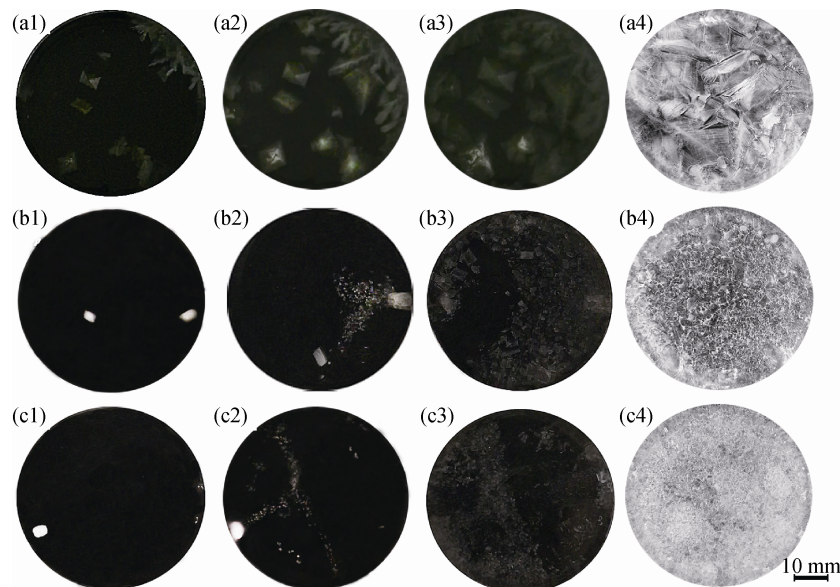


Fig. 5. Results of the physical simulation of crystallization under natural (a), V-vib (b), and H-vib conditions (c).

Figs. 5(b1) and 5(c1) show the position of the primary crystals, which mainly locate near the wall under either V-vib or H-vib conditions. During crystallization, a large amount of fine crystals are continuously separated from the primary crystals around the wall, forming free crystals, as shown in Figs. 5(b2) and 5(c2). Finally, the free crystals are dispersed evenly at each position of the liquid during vibration. As evident in Figs. 5(b4) and 5(c4), the sodium thiosulfate crystals mainly consisted of tiny homogeneous equiaxed crystals.

Because of the viscosity of the fluid, vibration of the culture dish wall can affect the adjacent liquid, causing the liquid to accelerate. As suggested by the fluid boundary layer concept proposed by Prandtl, the impact of vibration on the fluid can be limited to the thin layer near the object surface [22]. The inability of the wall to satisfy the non-slip

boundary condition results in nonzero relative tangential velocity, corresponding strong shear stress at the solid–liquid interface, and a narrow disturbance of the boundary layer with nonzero vorticity near the wall [23]. According to the Schlichting mechanism [24], the pulsing vortex generated within the boundary layer and the inhomogeneous tangential velocity are subjected to nonlinear reaction, causing the vortex to form within the boundary layer. When the vortex flows to the center of the liquid, it diffuses because of viscous interaction. By contrast, viscous transport can always reduce the degree of nonuniformity of physical quantities' distributions, contributing to the equilibrium distribution of the vortex. That is, the vortex inside the liquid will dissipate and finally disappear because of the viscous effect. Therefore, the mechanical vibration can result in the disturbance of the boundary layer near the wall but the dis-

turbance is limited to this region.

A comparison of Figs. 5(b1) and 5(b2) reveals that, although the primary crystal in the liquid center moves with the convection under vibration, no free crystals appeared near the primary crystal. However, the primary crystal near the wall produces a large amount of free crystals. Moreover, because of the low and uniform liquid temperature, dendrite remelting is unlikely. Therefore, we deduced that the boundary layer near the wall is severely disturbed, which causes the crystal to separate from the primary crystal and form free crystals. These free crystals finally develop a crystalline morphology dominated by fine grains.

3.2.2. Effect of vibration on nucleation

Vibrational energy influences the final microstructure in two manners: the periodic stress and the forced convection in the molten alloy [25]. Both of the two manners can influence the nucleation and growth process of the solidified alloy. According to Ref. [26], the energy barrier ΔG for the crystal to nucleate on the substrate is

$$\Delta G = \frac{4\pi\gamma_{LC}^3 T_m^2}{3(\Delta H_m \Delta T)^2} (2 - 3\cos\theta + \cos^3\theta) \quad (1)$$

where T_m is the equilibrium melting temperature, ΔH_m is the latent heat of melting, ΔT is the undercooling below T_m , θ is the contact angle, and γ_{LC} is the surface energy of the liquid–crystal interface. If the liquid wets the substrate completely, the contact angle θ is zero and so is ΔG . Thus, the crystal can nucleate on the substrate without having to overcome any energy barrier required for nucleation. In this process of growth, the crystal that nucleates on the substrate will inevitably result in the redistribution of solute concentration in front of the solid–liquid interface in the liquid metal, thereby reducing the solidifying point of the interface front as well as the undercooling in the liquid metal. The higher degree of solute segregation is accompanied by a lower undercooling and growth rate. Because the root of the crystal nucleus is adjacent to the substrate grain and because the solute has the worst diffusion conditions in this region, the degree of segregation is most serious at the root of the nucleus, which strongly inhibits the crystal's growth. Furthermore, other parts farther from the root can be easily homogenized through both diffusion and convection. Therefore, the parts are subjected to greater undercooling and are characterized by a higher growth rate. For the aforementioned reasons, the crystal nuclei can be necked at the corresponding roots at the initial stage of solidification, forming shapes with large heads but small roots, referred to as necked crystals, as shown in Fig. (6).

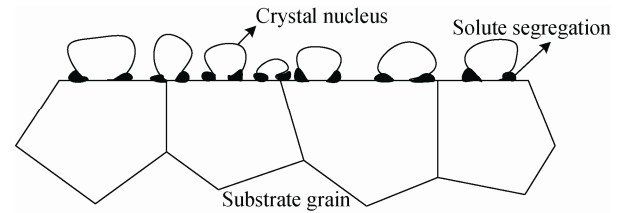


Fig. 6. The necked crystal nuclei.

According to the principle of similarity, the mechanical vibration can also produce a disturbance of the boundary layer around the fusion line. Compared with the vibration at the weld pool center, that on the fusion line is more intense and the shear force is greater at the fusion line because of the disturbance of boundary-layer existence. In addition, the liquid-metal temperature in the weld pool is possibly high enough to melt the crystal roots. Consequently, the necked crystals are susceptible to detachment. Under the combined action of the boundary-layer disturbance and necking, the mechanical vibration can cause the crystals to detach from the substrate, forming free crystals in the nucleation stage of the weld pool.

Thereafter, the free crystals move with the vibration-induced convection of the liquid metal. Because the temperature of the liquid metal in the weld pool is inhomogeneous, the free crystals can remelt and disappear when they are subjected to the high-temperature liquid. Conversely, the free crystals can remain and form new crystal nuclei, which will promote grain refinement when they encounter the low-temperature liquid. Therefore, we deduced that the amount of free crystals retained in the weld pool determines the degree of refinement.

3.2.3. Effect of vibration on free crystals' convection

The microstructures of the edges and centers of welds formed under vibration conditions are shown in Figs. 7 and 8, respectively. Figs. 7(a) and 8(a) show that the fusion zone under V-vib is mainly composed of fine equiaxed grains. However, a small number of columnar grains still exist in the upper part of the fusion zone. Figs. 7(b) and 8(b) show that the effect of grain refinement is obvious in the fusion zone under LFH-vib and that the fine grains near the fusion line restrain the growth of columnar crystals, which makes the phenomenon of epitaxial growth not obvious. As shown in Figs. 7(c) and 8(c), the microstructure of the weld center under TFH-vib is mainly composed of coarse and inhomogeneous equiaxed grains; however, the microstructure near the fusion line is still composed of coarse columnar grains.

The characteristics of the aforementioned morphology are related to the convection diversity of the weld pool with vibration modes. The form of Marangoni convection in the weld pool is shown in Fig. 9. Because Inconel 601H alloy

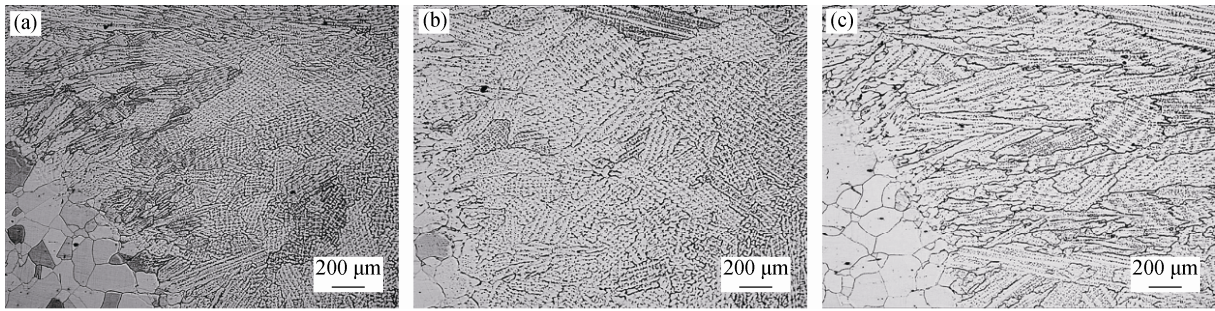


Fig. 7. Microstructures of the weld edges with 0.2 mm amplitude: (a) V-vib; (b) LFH-vib; (c) TFH-vib.

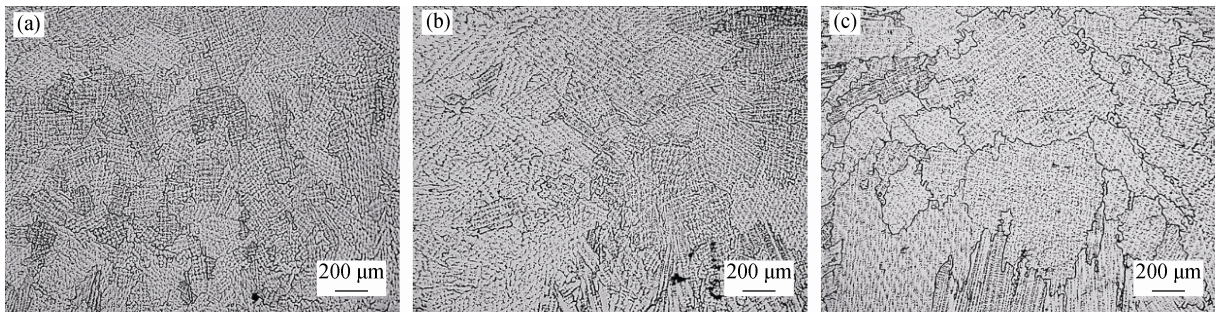


Fig. 8. Microstructures of weld centers with 0.2 mm amplitude: (a) V-vib; (b) LFH-vib; (c) TFH-vib.

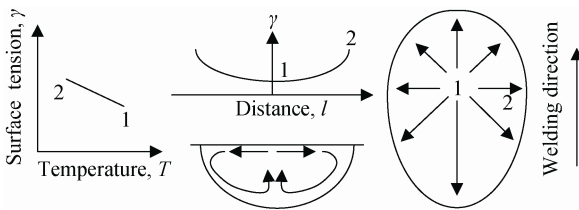


Fig. 9. The Marangoni convection of the weld pool.

without surface-active agent, the warmer liquid metal of lower surface tension near the center of the pool surface is pulled outward by the cooler liquid metal of the higher surface tension at the pool edge. Free crystals disperse with the Marangoni convection, and these crystals can be melted by the high temperature. However, when the fluid is subjected to mechanical vibration, the vibration can produce additional effects on Marangoni convection. The physical simulation shows that the movement of free crystals is mainly caused by vibration. Therefore, vibration is reasonably expected to play an important role in the convection of the liquid.

In the V-vib-assisted welding, the weld is mainly subjected to the reciprocating movement in a direction perpendicular to the platform. Therefore, liquid in the weld pool exhibits a trend of upward movement. With the combined action of the V-vib and Marangoni convection, high-temperature liquid metal in the center of weld pool is accelerated to move to the surface of weld pool. At the same time, the high temperature liquid metal at the surface of weld pool moves to the edge of weld pool under the driving

force of surface tension, which causes a part of free crystals to remelt and disappear. Thus, in the upper part of the fusion line, the grain refinement effect is poor and even columnar grains exist in this region, as shown in Fig. 7(a). However, the temperature near the bottom of the weld pool is low, enabling free crystals to survive and grow. The vibrational energy can provide sufficient heat exchange at the center of the weld pool to decrease the temperature gradient and increase the component supercooling zone in this region. Therefore, the free crystals can form fine equiaxed grains at the center of the weld pool, as shown in Fig. 8(a).

In the LFH-vib-assisted welding, the Marangoni convection will be disturbed by the reciprocating movement in the direction parallel to the weld length. Thus, the additional energy generated by the mechanical vibration weakens the convection effect from the center to the edge of the weld pool. The remelting effect of high-temperature liquid is reduced, and the free crystals' retention rate near the fusion line increases greatly. Therefore, significant grain refinement near the fusion line inhibits the phenomenon of epitaxial growth, as shown in Fig. 7(b).

In the TFH-vib-assisted welding, vibration caused the liquid metal to produce reciprocating movement in the direction perpendicular to the weld length. Under this vibration mode, the high temperature liquid metal in the center of weld pool flow to the fusion line, so that the free crystals are remelted. Thus, the columnar grains near the fusion line begin to grow as shown in Fig. 7(c). Due to the sufficient heat

exchange caused by mechanical vibration, the temperature gradient of the center of the weld pool gradually flattens. The residual crystals in liquid metal can grow up in the form of coarse equiaxed grains, as shown in Fig. 8(c).

Fig. 10 shows the microstructures of the heat-affected zone (HAZ) of Inconel 601H alloy welds formed without and with vibration. In the conventional GTAW process, as shown in Fig. 10(a), the HAZ is narrow and grain coarsening is not obvious. Compared with the width of the HAZ in the GTAW process, that in the vibration-assisted welding processes is substantially greater, as shown in Figs. 10(b)–10(d), where the width of HAZs is increased to ap-

proximately 866 μm , 877 μm , and 1054 μm , respectively. The increase in HAZ width also demonstrates that the vibration caused the accelerated convection of liquid metal, which led to a longer holding time of high temperature in the HAZ. The maximum width of the HAZ in the TFH-vib process is mainly attributable to the vibration causing the liquid metal to flow to the fusion line directly. In this situation, the HAZ has the longest holding time at high temperature. In addition, vibration-assisted welding resulted in a substantial increase in the width of the HAZ, which is not helpful for improving the hot cracking susceptibility of the HAZ.

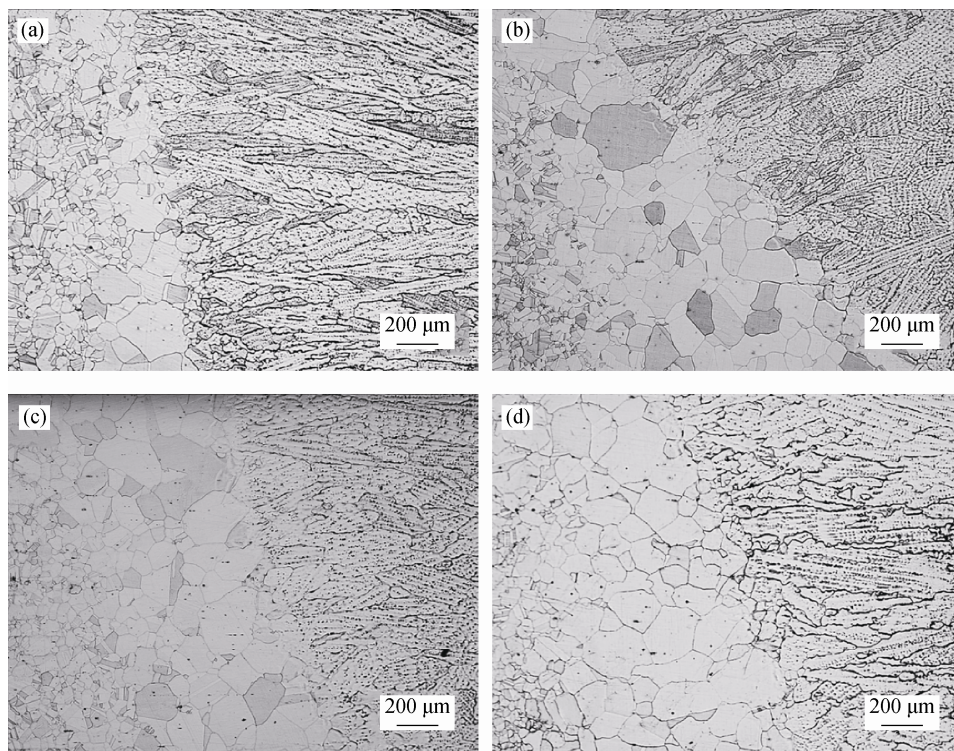


Fig. 10. Microstructures of the HAZ with 0.2 mm amplitude: (a) GTAW; (b) V-vib; (c) LFH-vib; (d) TFH-vib.

In summary, substantial grain refinement was achieved in Inconel 601H alloy welds by low-frequency-mechanical-vibration-assisted GTAW. The main mechanism of grain refinement is the formation of free crystals. The low-frequency mechanical vibration induces severe nonlinear disturbance of the boundary layer around the fusion line, causing the necks of crystal nuclei to detach from the substrate grains at the nucleation stage of solidification, disperse with the convection of liquid metal, and consequently form free crystals. These free crystals can result in grain refinement in the weld pool. Because different vibration modes result in different numbers of free crystals in the weld pool, the degree of grain refinement of welds under different vibration modes differs.

3.3. Precipitation phase and segregation

The distribution of the precipitation phase is shown in Fig. 11. The XRD analysis results shown in Fig. 12, combined with the EDS analysis results shown in Figs. 13(a) and 13(b), demonstrates that the tiny and coarse precipitation phase are the γ' phase and a Ti(C,N) compound, respectively. Reflections associated with the Ti(C,N) compound are not observed in the XRD pattern in Fig. 12 because of its low concentration. The γ' phase is an important strengthening phase in Inconel 601H alloy; the main component of the alloy is $\text{Ni}_3(\text{Al,Ti})$ [27]. The EDS analysis of the chemical composition of the matrix phase is included in Fig. 13(c) for reference.

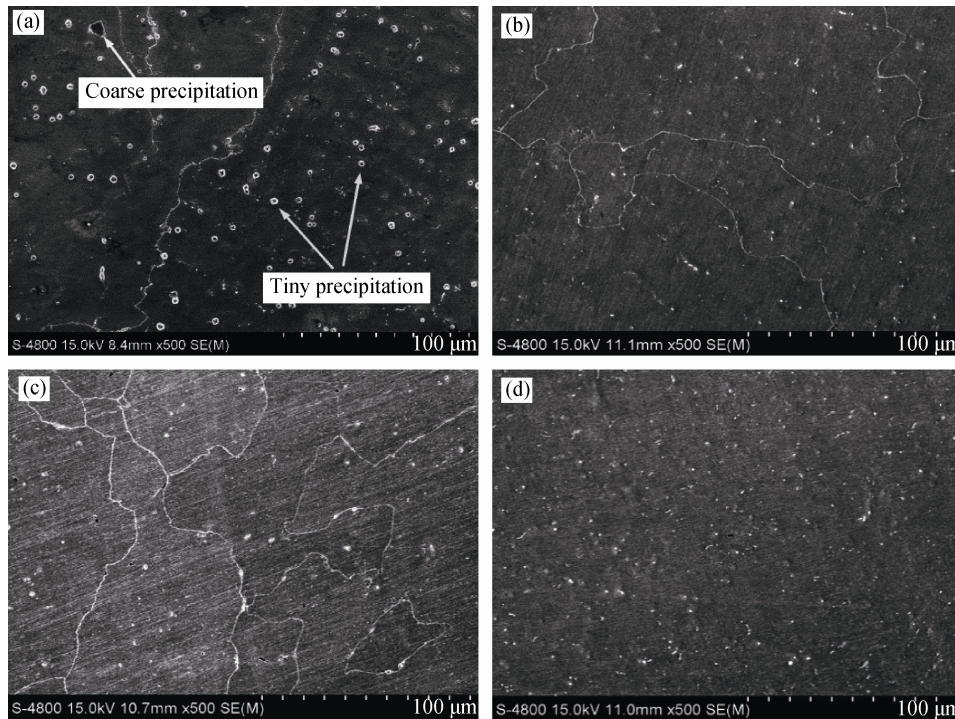


Fig. 11. Scanning electron micrographs of Inconel 601H alloy welds with 0.2 mm amplitude: (a) conventional GTAW; (b) V-vib; (c) LFH-vib; (d) TFH-vib.

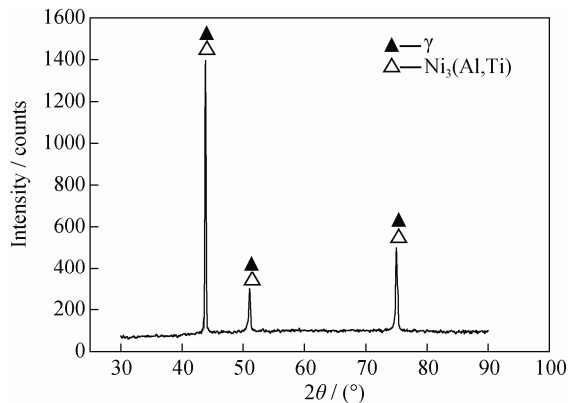


Fig. 12. XRD pattern of the Inconel 601H alloy matrix phase.

In the GTAW process, as evident in Fig. 11(a), the γ' phase nucleates and coarsens along coarse columnar grains. By contrast, analysis of the welds obtained by vibration-assisted welding shows that the γ' phase becomes finer while simultaneously exhibiting a dispersed homogeneous distribution, as shown in Figs. 11(b)–11(d). The characteristics of the γ' phase distribution can hinder the movement of dislocations and improve the mechanical properties of materials at high temperatures. In addition, Figs. 11(b) and 11(c) show extensive γ' phase pinning on grain boundaries, which have been strengthened.

The mass fraction distribution of Ti in the weld under vibration is shown in Fig. 14. Ti is an important compo-

nent of the γ' phase, which is a substantial constituent of liquid films [28–29]. The liquid film is one of the important factors influencing the initiation of hot cracking. In this study, vibration-assisted welding was found to effectively promote the fine and uniform distribution of γ' phase, as shown in Fig. 11. Also, the segregation of Ti in the weld can be reduced, as shown in Fig. 14. In Fig. 14(a), the peak value of the Ti mass fraction reaches approximately 14% in the center of the weld formed using GTAW. However, as shown in Figs. 14(b)–14(d), the peak value of the Ti mass fraction in the weld center of the welds formed under V-vib, LFH-vib, and TFH-vib conditions decreases to approximately 4%, 7%, and 8%, respectively. Thus, vibration-assisted welding reduces the segregation of the weld center. This effect is likely related to the refinement and uniform distribution of the γ' phase in the weld. In addition, the peak value of the Ti mass fraction in the weld center is much higher than that in the region near the fusion line without vibration, as shown in Fig. 14(a). This result is mainly attributed to the coarse columnar grains in the weld center. However, in the welds formed under V-vib and LFH-vib conditions, the microstructures of the whole fusion zone are more uniform and finer. At the same time, no significant difference is observed in the peak value of the Ti mass fraction between the weld center and the fusion line, as shown in Figs. 14(b) and 14(c). Although the microstructure of the fusion zone in the

TFH-vib weld is inhomogeneous, the difference of the peak value of Ti mass fraction between the weld center and the fusion line is also not obvious. Therefore, the vibra-

tion-assisted welding processes reduce Ti element segregation, mainly because vibration accelerates liquid metal convection, resulting in the uniform distribution of the solute.

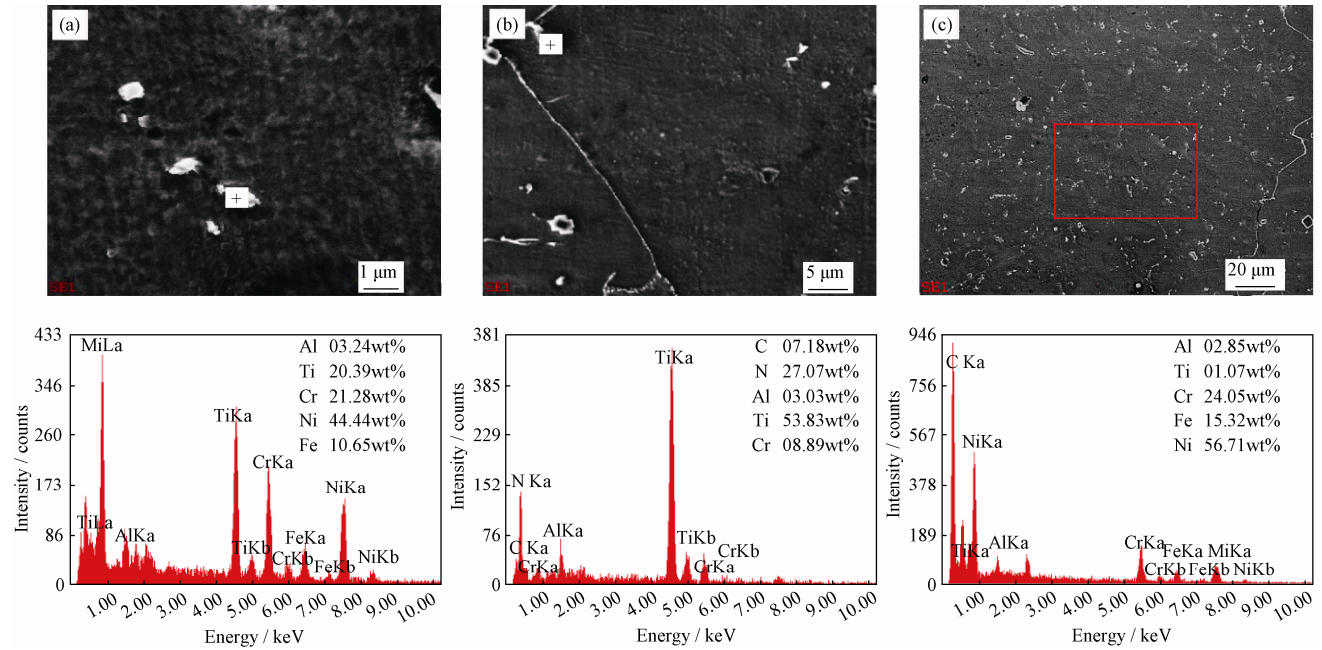


Fig. 13. EDS analyses: (a) the γ' phase; (b) the Ti (C,N) compound; (c) the matrix phase.

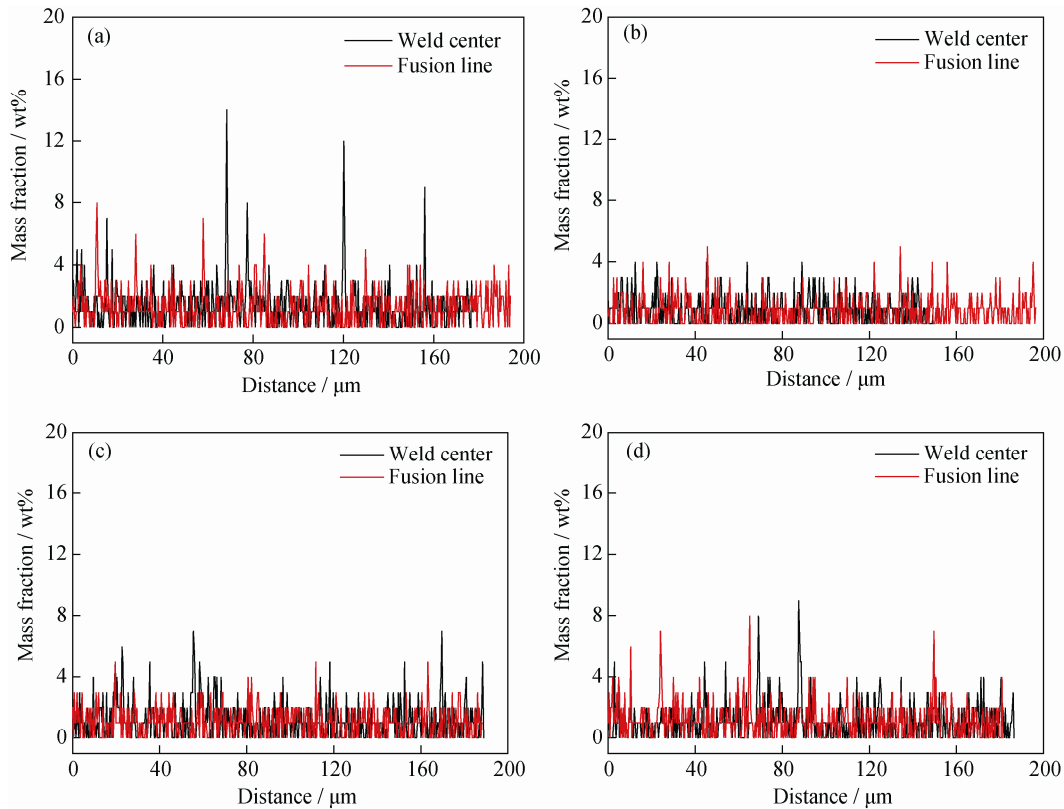


Fig. 14. Ti mass fraction distribution in the weld with 0.2 mm amplitude: (a) conventional GTAW; (b) V-vib; (c) LFH-vib; (d) TFH-vib.

The larger and continuous grain boundary promotes an increase in liquid films' continuity, and a coarse γ' phase also increases the thickness of the liquid film, as shown in Fig. 11(a). In these cases, strain accumulation during the solidification process can make the grain boundary more susceptible to cracking initiation. By contrast, the finer and more uniform equiaxed grains obtained by vibration provide more grain boundary area, allowing strain to be more readily accommodated, thereby reducing the unit strain for a given grain boundary. The dispersed γ' phase can improve the grain-boundary strength, which in turn reduces the potential for grain-boundary sliding and crack initiation. In addition, the Ti is the major segregation element that forms the γ' phase, and the more homogeneous Ti distribution observed in Fig. 14 decreases the segregation, which is also helpful to suppress the generation of hot cracking of the nickel-based alloys.

3.4. Hardness distribution

The hardness of the vibration-assisted weld joints is shown in Fig. 15. On the whole, the base-metal hardness is the highest. Because the grains become coarse and the precipitation phases are dissolved into the matrix at high temperatures, the HAZ exhibits the lowest hardness. The hardness distribution of the GTAW joint fluctuates greatly, which is mainly related to the coarse grain and inhomogeneous microstructure.

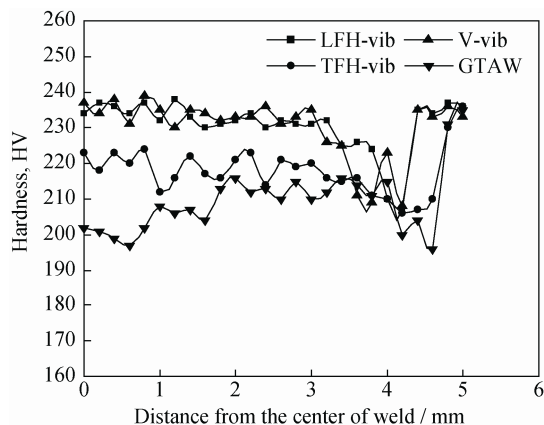


Fig. 15. Hardness of Inconel 601H alloy vibration-assisted weld joints.

Compared to the GTAW process, the V-vib and LFH-vib processes substantially improve the hardness of the weld. In addition, the hardness distribution of the fusion zone is steady, which is likely related to the fine grain strengthening caused by the fine and uniform microstructure. However, the increase in the width of the HAZ results in a corresponding increase of the low-hardness range of the HAZ.

Although the hardness of the weld center under TFH-vib is improved, the overall hardness of the fusion zone is relatively low, and great fluctuation is observed in the hardness distribution.

The hardness of the welding joints abruptly changes in the GTAW process, which can lead to stress concentration and the crack initiation. The V-vib- and LFH-vib-assisted welding can effectively solve this problem and improve the mechanical properties of the welding joints. However, the TFH-vib-assisted welding joint has coarse grains and an inhomogeneous microstructure, resulting in greater fluctuation in the hardness distribution. Therefore, this vibration mode has limited ability to improve the mechanical properties of the welding joint.

4. Conclusions

(1) Significant grain refinement could be achieved in Inconel 601H alloy welds by vibration-assisted GTAW. The main nucleation mechanism was that vibration promoted the generation of a large number of free crystals in the nucleation stage.

(2) In terms of the effect of grain refinement of welds, a threshold value of vibration amplitude was closely related to the vibration mode. Different vibration modes led to different grain refinement effects, which was mainly attributed to the difference in convection induced by the vibration.

(3) Fine equiaxed grains and dispersed γ' phase could enhance the grain-boundary strength of the alloy and are beneficial in preventing the initiation of hot cracking during welding of nickel-based alloys. However, the vibration-assisted welding dramatically increased the width of the HAZ, which was unfavorable for improving the hot-cracking susceptibility of the HAZ.

(4) The V-vib and LFH-vib could enhance the hardness of the welding joints, and the hardness distribution of the fusion zone was stable. However, the hardness distribution of the fusion zone fluctuated greatly with TFH-vib.

Acknowledgements

The authors gratefully acknowledge the financial supported by the Natural Science Foundation of Hebei Province, China (No. E2017202011).

References

- [1] J.C. Lippold, S.D. Kiser, and J.N. Dupont, *Welding Metallurgy and Weldability of Nickel-Base Alloys*, John Wiley & Sons,

- New Jersey, 2009, p. 100.
- [2] Y. Sharir, J. Pelleg, and A. Grill, Effect of arc vibration and current pulses on microstructure and mechanical properties of TIG tantalum welds, *Met. Technol.*, 5(1978), No. 1, p. 190.
- [3] B.B. Wei, Unidirectional dendritic solidification under longitudinal resonant vibration, *Acta Metall. Mater.*, 40(1992), No. 10, p. 2739.
- [4] Y. Cui, C.L. Xu, and Q.Y. Han, Microstructure improvement in weld metal using ultrasonic vibrations, *Adv. Eng. Mater.*, 9(2010), No. 3, p. 161.
- [5] S.P. Tewari and A. Shanker, Effects of longitudinal vibration on tensile properties of weldments, *Weld. J.*, 73(1994), No. 11, p. 272.
- [6] A.S.M.Y. Munsif, A.J. Waddell, and C.A. Walker, Modification of welding stresses by flexural vibration during welding, *Sci. Technol. Weld. Joining*, 6(2001), No. 3, p. 133.
- [7] T. Watanabe, M. Shiroki, A. Yanagisawa, and T. Sasaki, Improvement of mechanical properties of ferritic stainless steel weld metal by ultrasonic vibration, *J. Mater. Process. Technol.*, 210(2010), No. 12, p. 1646.
- [8] C.W. Kuo, C.M. Lin, G.H. Lai, Y.C. Chen, Y.T. Chang, and W.T. Wu, Characterization and mechanism of 304 stainless steel vibration welding, *Mater. Trans.*, 48(2007), No. 9, p. 2319.
- [9] B.P. Pearce and H.W. Kerr, Grain refinement in magnetically stirred GTA welds of aluminum alloys, *Metall. Mater. Trans. B*, 12(1981), No. 3, p. 479.
- [10] X.B. Liu, F.B. Qiao, L.J. Guo, and X.E. Qiu, Metallographic structure, mechanical properties, and process parameter optimization of 5A06 joints formed by ultrasonic-assisted refill friction stir spot welding, *Int. J. Miner. Metall. Mater.*, 24(2017), No. 2, p. 164.
- [11] L. Shi, C.S. Wu, and X.C. Liu, Modeling the effects of ultrasonic vibration on friction stir welding, *J. Mater. Process. Technol.*, 222(2015), p. 91.
- [12] W.L. Dai, Effects of high-intensity ultrasonic-wave emission on the weldability of aluminum alloy 7075-T6, *Mater. Lett.*, 57(2000), No. 16-17, p. 2447.
- [13] X.C. Liu and C.S. Wu, Material flow in ultrasonic vibration enhanced friction stir welding, *J. Mater. Process. Technol.*, 225(2015), p. 32.
- [14] X.C. Liu and C.S. Wu, Elimination of tunnel defect in ultrasonic vibration enhanced friction stir welding, *Mater. Des.*, 90(2016), p. 350.
- [15] S. Kou and Y. Le, Improving weld quality by low frequency arc oscillation, *Weld. J.*, 1985, p. 51.
- [16] W.T. Wu, Influence of vibration frequency on solidification of weldments, *Scripta Mater.*, 42(2000), No. 7, p. 661.
- [17] T. Yuan, Z. Luo, and S. Kou, Grain refining of magnesium welds by arc oscillation, *Acta Mater.*, 116(2016), p. 166.
- [18] R.H. Mathiesen, L. Arnberg, P. Bleuet, and A. Somogyi, Crystal fragmentation and columnar-to-equiaxed transitions in Al-Cu studied by synchrotron X-Ray video microscopy, *Metall. Mater. Trans. A*, 37(2006), No. 8, p. 2515.
- [19] D. Ruvalcaba, R.H. Mathiesen, D.G. Eskin, L. Arnberg, and L. Katgerman, In situ observations of dendritic fragmentation due to local solute-enrichment during directional solidification of an aluminum alloy, *Acta Mater.*, 55(2007), No. 13, p. 4287.
- [20] A. Hellawell, S. Liu, and S.Z. Lu, Dendrite fragmentation and the effects of fluid flow in castings, *JOM*, 49(1997), No. 3, p. 18.
- [21] T. Yuan, Z. Luo, and S. Kou, Mechanism of grain refining in AZ91 Mg welds by arc oscillation, *Sci. Technol. Weld. Joining*, 22(2017), No. 2, p. 97.
- [22] J.R. Welty, C.E. Wicks, R.E. Wilson, and G.L. Rorrer, *Fundamentals of Momentum, Heat, and Mass Transfer*, 5th Ed., John Wiley & Sons, New Jersey, 2007, p. 144.
- [23] L.X. Zhuang, X.Y. Yin, and H.Y. Ma, *Fluid Mechanics*, University of Science and Technology of China Press, HeFei, 1991, p. 321.
- [24] H. Schlichting and K. Gersten, *Boundary-Layer Theory*, McGraw-Hill Book Company, New York, 1979, p. 24.
- [25] J. Campbell, Effects of vibration during solidification, *Int. Metall. Rev.*, 26(1981), No. 1, p. 71.
- [26] S. Kou, *Welding Metallurgy*, 2nd Ed., John Wiley & Sons, New Jersey, 2003, p. 170.
- [27] S.S. Ao, Zhen Luo, P. Shan, and W.D. Liu, Microstructure of inconel 601 nickel-based superalloy laser welded joint, *Chin. J. Nonferrous Met.*, 25(2015), No. 8, p. 2099.
- [28] A.R.P. Singh, S. Nag, J.Y. Hwang, G.B. Viswanathan, J. Tiley, R. Srinivasan, H.L. Fraser, and R. Banerjee, Influence of cooling rate on the development of multiple generations of γ' precipitates in a commercial nickel base superalloy, *Mater. Charact.*, 62(2011), No. 9, p. 878.
- [29] O.A. Ojo and M.C. Chaturvedi, On the role of liquated γ' precipitates in weld heat affected zone microfissuring of a nickel-based superalloy, *Mater. Sci. Eng. A*, 403(2005), No. 1-2, p. 77.